Parameter Sensitivity for Wave-Breaking Closures in Boussinesq-Type Models

Subodh Joshi, M. Kazolea, Mario Ricchiuto

Parameter sensitivity for wave breaking closures in Boussinesq-type models

S. M. Joshi[b] M. Kazolea[a] and M. Ricchiuto[a]
[a] INRIA, Univ. Bordeaux, CNRS, Bordeaux INP, IMB, UMR 5251, 200 Avenue de la Vieille Tour, 33405 Talence cedex, France
[b] Department of Computational and Data Sciences, Indian Institute of Science, C. V. Raman Rd, Bangalore, Karnataka, India, 560012

Abstract

We consider the issue of wave-breaking closure for the well known Green-Naghdi model and attempt at providing some more understanding of the sensitivity of some closure approaches to the numerical set-up. More precisely and based on [16] we used two closure strategies for modelling wave-breaking of a solitary wave over a slope. The first one is the hybrid method consisting of suppressing the dispersive terms in a breaking region and the second one is an eddy viscosity approach based on the solution of a turbulent kinetic energy model. The two closures use the same conditions for the triggering of the breaking mechanisms. Both the triggering conditions and the breaking models themselves use case depended / ad/hoc parameters which are affecting the numerical solution wile changing. The scope of this work is to make use of sensitivity indices computed by means of Analysis of Variance (ANOVA) to provide the sensitivity of wave breaking simulation to the variation of parameters such as the mesh size and the breaking parameters specific to each breaking model. The sensitivity analysis is performed using the UQlab framework for Uncertainty Quantification [24].

Key words: keywords

Contents

1 Introduction

The solitary wave run up and run down over a slope is a classical hydrodynamic problem. It is highly relevant for the investigation of the characteristics of Tsunami waves, since solitary waves model some of the important aspects of Tsunami waves. We refer the readers to a series of works investigating the physics of solitary waves' propagation including shoaling, breaking and run up over a slope, by either an analytical approach (e.g [35]) or by simulations , see e.g. [12, 13, 20, 21, 35, 41] and references therein. Among the various available mathematical models for Tsunami waves' propagation depth-averaged approaches enjoy a wide popularity thanks to their ability to describe the physics with computational ease. The Boussinesq type (BT) models, which typically incorporate frequency dispersion, have been also used to study the physics of solitary waves, see for example [26, 28, 41]. Moreover, the propagation, breaking and run-up of solitary waves is a classical test case for the validation and calibration of BT models, see [11, 31, 36, 37] among others.

When using BT models, the treatment of wave-breaking necessitates deploying a wave-breaking closure model/mechanism in the surf zone in order to account for the dissipative dynamics associated with it. We can generally say that we can distinguish the wave-breaking treatment in three main categories. The hybrid models, the roller models and the eddy viscosity models. The philosophy of the wave-breaking closures is to mimic the energy dissipation either by adding extra terms to the equations (roller models and eddy viscosity models) or by a local coupling of the dispersive propagation model with the shallow water equations. In the later approach, the non linear shallow water equations (NSWE) are solved in the breaking regions, with the breaking wave modeled as a shock so that the total energy is dissipated. We have to be aware that all the wave-breaking closures introduce coefficients/parameters which need to be calibrated with experimental/analytical data. We also have to keep in mind that the calibration methodology may be specific to a particular set of equations. Extensive reviews on wave-breaking closures for BT models can be found in [15, 16] and [6].

The work of Zelt [39] is one of the earliest works that included a simple eddy viscosity wave-breaking mechanism into a Lagrangian finite element Boussinesq wave model to treat the wave-breaking, as well as study the run-up and breaking of solitary waves. In that work, a simple parameter analysis and calibration of the breaking model was performed, which in turn used the work of Synolakis [35]. Later, Grilli et al. [12] examined breaking and non breaking waves on a range of slopes using a fully non-linear potential flow model, with particular attention paid to the criterion that distinguishes breaking and non-breaking waves, and breaking indices. Zhou et al. [41] performed a parametric investigation of breaking solitary wave over fringing reefs using the weakly nonlinear weakly dispersive equations of Nwogu [27], and the hybrid wave-breaking closure. A more recent work that also performs parametric studies of solitary wave propagation and run-up over fringing reefs is the one of Ning et al. [26]. They use a fully non linear Boussinesq wave model with the hybrid wave-breaking closure. However, they don't account for the parameters of the breaking model.

Recently in [16] the authors considered the issue of wave-breaking closure when using weakly dispersive Boussinesq propagation models. They focused on the enhanced equations of Nwogu [27] and the enhanced equations of Green-Naghdi (GN) [5, 11], and considered two different wave-breaking closures. The first one being the hybrid closure proposed in [37] and the second one being an eddy viscosity approach based an adaptation of the turbulent kinetic energy (TKE) proposed by Nwogu [29]. The results clearly showed a reduced sensitivity to the mesh size when using the TKE eddy viscosity closure compared

to the hybrid closure model. The above models also present a dependency on the parameters of the detection criteria, as well as on the coefficients of the TKE equation. The scope of this work is to quantify the sensitivity of these parameters when using the Green Naghdi equations. To this end, the use of a set up allowing full control of the initial/free stream data is of paramount importance to avoid uncertainties in the incoming wave to interfere with those related to the breaking closure. This further justifies the choice of the solitary wave as an incoming state, for its inherent simplicity and robustness.

The paper is organized as follows. Section 1 discusses briefly the propagation model, and its numerical solution. Section 2 presents the two different wave-breaking closures used in this work. Section 3 discusses briefly the sensitivity analysis model used to perform the parameter sensitivity analysis. The numerical experiment and the results of the analysis, for both approaches, are presented in Section 4. Section 5 presents a summary of the results and a comparison of the two breaking models. The paper ends with conclusions and an outlook of the future developments.

2 Green-Naghdi wave model and its numerical discretization

The GN equations model the propagation of weakly non-linear fully dispersive waves. The range of validity of the model all the range of values of the nonlinearity parameter $\epsilon = A/h_0$ (amplitude over depth at rest), but it requires that the shallowness parameter $\mu = h_0/\lambda$ (depth at rest over wavelength) to be small, so that μ^4 effects are neglected. The equations have the form:

$$\begin{aligned} h_t + (hu)_x &= 0 \\ (hu)_t + (hu^2)_x + gh\eta_x + \alpha\mathcal{T}((hu)_t + (hu^2)_x + gh\eta_x) &= F_{br} + F_m \end{aligned} \tag{1}$$

h being the water height, u the velocity, d the still water level, b the topography function, and F_m is the bottom friction. F_{br} accounts for the extra breaking terms, activated only when an eddy viscosity breaking closure is used. In the above system we have also defined $\mathcal{W} = g\mathcal{T}(d\eta_x)$ and $\mathcal{R} = h\mathcal{Q}(u)$, where $\mathcal{T}(\cdot)$ and $\mathcal{R}(\cdot)$ are the linear operators given as:

$$\mathcal{T}(\cdot) = -\frac{1}{3}h^2(\cdot)_{xx} - \frac{1}{3}hh_x(\cdot)_x + \frac{1}{3}\left[h_x^2 + hh_{xx}\right](\cdot) + \left[b_xh_x + \frac{1}{2}hb_{xx} + b_x^2\right](\cdot) \tag{2}$$

$$\mathcal{Q}(\cdot) = 2hh_x(\cdot)_x^2 + \frac{4}{3}h^2(\cdot)_x(\cdot)_{xx} + b_xh(\cdot)_x^2 + b_{xx}h(\cdot)(\cdot)_x + \left[b_{xx}h_x + \frac{1}{2}hb_{xxx} + b_xb_{xx}\right](\cdot)^2 \tag{3}$$

Following our previous work, we discretize the equations in time with a splitting in which we start by integrating the non-dissipative equations in the form proposed in [11] :

$$\begin{aligned} h_t + (hu)_x &= 0 \\ (hu)_t + (hu^2)_x + gh\eta_x &= \phi \\ (I + \alpha\mathcal{T})\,\phi &= \mathcal{W} - \mathcal{R} \end{aligned} \tag{4}$$

and then we add an implicit update for the velocity of the form

$$h^{n+1}u^{n+1} = h^nu^* + \Delta tF_{br}(h^{n+1}, u^{n+1}) + F_m(h^{n+1}, u^{n+1}) \tag{5}$$

which is solved by some iterative technique, and where u^* and h^{n+1} obtained from (4). Concerning the latter, we solve it in two independent steps. First the elliptic equation is solved for the non-hydrostatic term ϕ, then the hyperbolic equations for h and hu are evolved. We implement a standard C^0 Galerkin

finite element approximation for the elliptic step and a high order finite volume method for the hyperbolic one. More precisely we use a third order MUSCL scheme for the reconstruction of the variables. The approximate Riemann solver of Roe [30] is used to evaluate the numerical fluxes at the interfaces. We also use an upwind discretization of the topography source. The discretized term ϕ is the link between the two steps and is integrated exactly over the cell C_i. A conservative computation of wet/dry fronts is used resulting in a well-balanced scheme. The time integrator that we use is the Adams-Bashforth/Adams Moulton predictor corrector scheme. We refer to [11, 16] for more details.

3 Wave breaking closures

A wave breaking closure can be distinguished in two steps. The first one is the detection of the breaking wave in time and in space, including both an initiation and/or termination trigger. The second important aspect is an energy dissipation mechanism. The wave breaking trigger models can be classified to phase averaged and phase resolving models. The phase averaged models use wave characteristics which are representative of one wave's phase and its more difficult to compute locally, while phase resolving models use local information of the wave. The last ones rely on a wave-by-wave analysis and are more efficient to program in the context of phase resolved simulations, see the recent work [1, 9] and [2] on breaking onset criteria. For the triggering mechanism, in this work, we use a combination of local and non-local criteria proposed in [15] and used also in [11, 16]. Each one is computed and checked in each cell of our mesh and if one of them is satisfied then the cell is flagged as a breaking cell. The criteria are the following:

1. the surface variation criterion, satisfied if $|\eta_t| \geq \gamma\sqrt{gh}$;
2. the local slope angle criterion, satisfied if $||\nabla\eta|| \geq \tan\theta$ with θ being a critical angle;
3. the Froude number criterion, requiring that $\mathrm{Fr} = \sqrt{H_{\max}\bar{H}}/H_{\min} > 1.3$. If this condition is not met, breaking is deactivated independently on the first two conditions.

The first criterion is activated as breaking starts on the front face of the wave. The second one acts complementary and is based on the critical front slope approach [33, 34]. This allows to flag steady hydraulic jumps while the first one is more efficient for moving fronts. In the last criterion $H_{\min\,/\,\max}$ are the depths in correspondence a wave's trough/peak, and $\bar{H}$ the average of the $\min$ and $\max$. The Froude criterion acts as a termination trigger. In practice, a wave by wave analysis is performed to flag cells containing breaking waves. Flagged cells are grouped according to the above local criteria, and form a breaking region which is enlarged to account for the typical roller length. For each breaking front peak and trough depths, $H_{\max}$ and $H_{\min}$ respectively, are computed. The reader can refer to previous works [1, 11, 15, 16, 36] for the details in the implementation of the wave breaking criteria. The first two criteria involve the dimensionless parameter γ and the critical angle θ, respectively, which are crucial for the flagging, and for which, to the authors knowledge, there is no general parametrisation.

3.1 Energy dissipation via bore capturing (hybrid wbc)

A common approach to deal with wave breaking for Boussinesq-type models , here referred to as the hybrid wave breaking closure (wbc) technique, relies on the deactivation of all the dispersive terms in the flagged region. This reduced the model to the shallow water equations, which exhibits the formation of a bore (or of a hydraulic jump) quite rapidly in the breaking region. Across the discontinuity, the classical

Rankine-Hugoniot theory can be applied, and a net decrease in total energy is observed and can be readily estimated [4, 7]. In this closure there is no additional diffusion term and no tuning parameter, besides those already involved in the detection. On the other hand, it is known that at the interface of the closure region spurious oscillation may appear and grow as numerical dissipation is reduced using e.g. mesh refinement. This issue has been investigated in [1, 16].

3.2 Energy dissipation using PDE based eddy viscosity (TKE wbc)

One way to parametrize the effect of wave breaking is by the addition of an eddy viscosity term in the momentum equation [17, 29, 31]. This results in the explicit addition of the right hand side of the second equation in (5) of a dissipative term, of the form $\mathbf{F}_{br} = \partial_x(\nu_t h \partial_x u)$ where ν_t is the turbulent eddy viscosity. In this work we consider an approach similar to the one studied in [16], in which the eddy viscosity is determined from an additional partial differential equation for the generation and transport of turbulent kinetic energy in breaking waves. The added viscosity is written as:

$$\nu_t = C_\nu \sqrt{k_b}\ell_t$$

where ℓ_t is a turbulent length scale. Inspired by [40], we use a vertically averaged mixing length defined as $\ell_t = \kappa_b A$, where k_b is the kinetic energy of the propagating bore, A is the bore's initial amplitude and κ_b is a constant controlling the width and intensity of the breaking. For more details see [16]. Following the work of Nwogu [29], the turbulent kinetic energy for k_b is determined from a semi-empirical transport equation, with a source term for turbulent kinetic energy production by wave-breaking. Dropping the subscript b for simplicity, we write:

$$k_t + uk_x = \mathcal{D} + \mathcal{P} - \mathcal{E} \tag{6}$$

with $\mathcal{D},\ \mathcal{P},\ \mathcal{E}$ being diffusion, production and dissipation terms respectively.

$$\mathcal{D} = \sigma \nu_t k_{xx}, \quad \mathcal{E} = -C_\nu^3 \frac{k^{3/2}}{\ell_t} \tag{7}$$

The constant σ controls the smoothness of the TKE and hence of the breaking viscosity in the breaking region.

$$\mathcal{P} = B(t,x)\frac{\ell_t}{\sqrt{C_\nu^3}}(u^s)^{3/2} \tag{8}$$

The parameter $B(t,x)$ is the breaking flag, and is either 0 or 1 depending on the wave breaking criterion, while u_s is the velocity at the free surface, for the GN equations defined as

$$u_s = u - \left[\frac{\eta^2}{2} - \left(\frac{h^2}{6} - \frac{h(h-d)}{2}\right)\right] u_{xx} - \left[\eta - \left(\frac{h}{2} - d\right)\right](du)_{xx}. \tag{9}$$

The fully discrete distribution of the nodal values of the TKE is obtained by integrating Eq. (6) with a semi implicit approach. Before the predictor time step is applied to the Boussinesq model, the nodal TKEs are evolved by first applying an explicit Euler update involving the same third order MUSCL upwind discretization of the transport operator $(uk)_x$ used for the shallow water equations. To avoid spurious negative values in this phase, the min-mod limiter is applied [19]. The predicted values k_i^* are then corrected by diagonally semi-implicit relaxation iterations as :

$$\left(\frac{\Delta t}{\Delta x} + \frac{2\sigma\nu_{t,i}^n}{\Delta x}\right)(k_i^{m+1} - k_i^m) = \Delta x \frac{k_i^m - k_i^*}{\Delta t} + \sigma \nu_{t,i}^n \frac{k_{i+1}^m - 2k_i^m + k_{i-1}^m}{\Delta x} + \left(\frac{B\ell_{t,i}^2}{\sqrt{C_{nu}^3}} u_s^3\right)^n - C_\nu^3 \left(\frac{k_i^{3/2}}{\ell_{t,i}}\right)^n$$

with an initial condition $k^0 = k^*$. The number of relaxation iterations used in practice is 5.

4 Sensitivity Analysis Model

The Analysis of Variance (ANOVA), first proposed by Sobol et. al. [22, 23], is a powerful technique for global sensitivity analysis. Later, an improved algorithm was proposed by Saltelli et. al. to reduce the computational cost of ANOVA [32]. A comprehensive review of the global sensitivity analysis methods, including the ANOVA technique, is given by Iooss and Lemaítre in [3]. Here, we briefly describe the ANOVA method to find out Sobol indices, that characterize the sensitivity of the model output with respect to contribution of each of the input parameters. Consider $\mathbf{X} \in \Omega \subset \mathbb{R}^d,\ d \in \mathbb{N}$ to be a random variable and let $f(\mathbf{X}) \in L^2(\Omega)$ be a square integrable function on domain $\Omega = [0,1]^d$. ANOVA decomposition of f quantifies the variance of the function output in terms of the input parameters (or a combination of the input parameters), and is given as follows (see [3, 22] and the references therein).

$$f(\mathbf{X}) = f_0 + \sum_{1 \le i \le d} f_i(X_i) + \sum_{1 \le i < j \le d} f_{ij}\left(X_i, X_j\right) + ... + f_{12...d}\left(\mathbf{X}\right) \tag{10}$$

under the condition imposed by the following equation:

$$\int_0^1 f_{i_1,i_2,...,i_s}\left(x_{i_1}, ..., x_{i_s}\right) dx_{i_k} = 0, \quad 1 \le k \le s, \quad \{i_1, ..., i_s\} \subseteq \{1, ..., d\}. \tag{11}$$

Here, f_0 is the expected value of the function f, which is quantified by $\mathbb{E}[Y]$ for each random variable $Y = f(\mathbf{X})$. The univariate function $f_i(X_i) = \mathbb{E}[Y|X_i] - \mathbb{E}[Y]$ quantifies contribution due to each random variable $Y = f(\mathbf{X})$. The bivariate function $f_{ij}\left(X_i, X_j\right) = \mathbb{E}\left(Y|x_i, x_j\right) - F_0 - F_i - F_j$ quantifies the joint contribution of each pair of input parameters covering all possible combinations. Similarly, the rest of the terms quantify the higher-order effects. It is possible to get a similar decomposition of the variance of the function $f(\cdot)$ as follows [3],

$$Var(Y) = \sum_{i=1}^{d} D_i(Y) + \sum_{i<j}^{d} D_{ij}(Y) + ... + D_{12...d}(Y), \tag{12}$$

where, $D_i(Y) = Var[\mathbb{E}(Y|X_i)]$, $D_{ij}(Y) = Var[\mathbb{E}(Y|X_i, X_j)] - (D_i(Y) + D_j(Y))$ and so on for the higher order terms. This decomposition is known as ANOVA decomposition. Finally, the Sobol' indices are given as (refer [3, 22]),

$$S_i = \frac{D_i(Y)}{Var(Y)}, \quad S_{ij} = \frac{D_{ij}(Y)}{Var(Y)}, \quad \text{Higher Order Terms} \tag{13}$$

Further, the Total Order (TO) Sobol' indices combine the lower-order and higher-order terms and are given by:

$$S_{T_i} = S_i + \sum_{i<j} S_{ij} + \sum_{j \ne i, k \ne i, j<k} S_{ijk} + \quad \text{Higher Order Terms} \tag{14}$$

Note that two-parameters (as well as three-, four- etc.) interactions involving x_i are already accounted in S_i, the same way that three-parameters contributions to the variance are also hidden in the two-parameters contributions, and so on. For this reason, the sum of all the total indices usually larger than 1.

To perform the sensitivity analysis in this work we used the UQlab-The framework for Uncertainty Quantification [25]. More precisely, we use the sensitivity analysis module which contains the methods for global sensitivity analysis that quantitatively measure the importance of each input parameter. We construct a surrogate model (meta-model) of our computational model prior to the Sobol sensitivity analysis. The surrogate model is a functional approximation of our computational model and is faster to evaluate. It is constructed using a relatively small number of input parameters and corresponding output results from our computational model. This way, we reduce the total computational cost to a great extend. In this work we use the Kriging (or Gaussian process regression) metamodel. A review on Kriging metamodeling can be found in [10, 18]. The preliminary results of our analysis have been presented in [14].

5 Case study: propagation, breaking and runup of a solitary wave

We study a well known numerical experiment involving the propagation, breaking, and runup of a solitary wave over a slope (see sketch on Figure 1). It is based on the work of Synolakis [35], where solitary waves with various nonlinearities $\epsilon = A/h_0$ were studied experimentally and numerically. For simplicity, we only investigate the breaking and runup processes and their sensitivity to the different physical and model parameters. This already will provide a quite large spectrum of results and informations related to the closure models. The initial solution consists of a solitary wave of amplitude A, defined by

$$\eta(x) = A\,\mathrm{sech}^2(k(x - x0)), \quad u(x) = c\left(1 - \frac{h_0}{\eta(x)}\right) \tag{15}$$

with $k = \sqrt{\frac{3A}{(h_0+A)*h_0^2}}$, $c = \sqrt{g(h_0 + A)}$ and $h_0 = 1m$. The bathymetry has the form

$$b(x) = \begin{cases} \frac{-x}{s}, & \text{if } x \leq s \\ -1, & \text{elswere.} \end{cases} \tag{16}$$

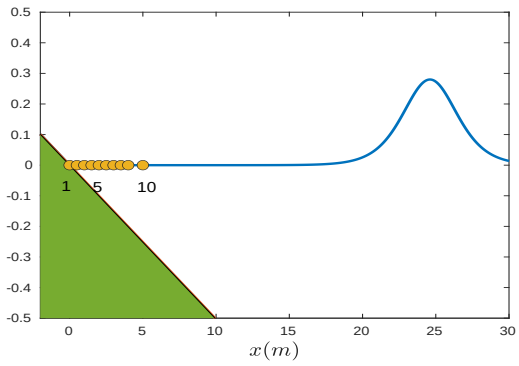

Figure 1: Initial conditions and position of the wave gauges.

The crest of the wave is placed offshore at $x_0 = s + \frac{1}{\rho}2.17832722$ with $\rho = \sqrt{3A/4h_0}$. The computational domain is $[-20, 80]m$ and the numerical parameters are constant and set to $\Delta x = 0.05$, cfl $= 0.1$. They are intentionally kept relatively small as to limit the numerical diffusion in the results. Figure 2 confirms that the computed solution, presented at time $6.4sec$ (i.e. already breaking), does not change as Δx

is refined and that we are still far from the fine mesh instabilities highlighted for the hybrid closure in [16]. We record time series of the surface elevation in 10 wave gauges every $0.5m$ from $x = 0$ to $x = 3.5$, plus two additional at $x = 4.0,$ and $5.0m$. In this spatial window, we have observed wave-breaking occurs for all the examined waves.

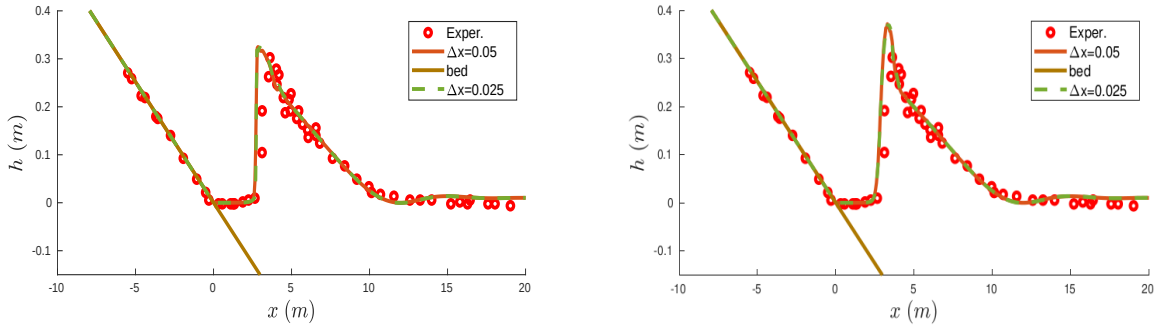

Figure 2: Computed solution, at early breaking for the hybrid(left) and the TKE (right) closures using $\Delta x = 0.05m$ and $\Delta x = 0.025m$.

We introduced uncertainties in both the model set up and the model parameters. In particular, wave amplitude, slope of the beach, and Manning friction coefficient are assumed to vary uniformly in the ranges $A \in [0.1,\ 0.6]$, slope $\in [-1/15,\ -1/25]$, $Nm \in [0.009,\ 0.075]$ respectively. All of the possible combinations of these parameters cover most of the practical scenarios. Uncertainty is introduced also in all the parameters of the breaking models.

For completeness, Figure 3 shows the evolution of the free surface, compared to the experimental data of [35], computed in the deterministic setting: slope $= -1/19.85$, $A = 0.28$, $Nm = 0.01$. For these computations, the wave breaking closure models have been parametrized using values proposed in literature [11, 16, 37]: $\gamma = 0.6$, $\theta = 0.53$ and $C_v = 10$ $\kappa_b = 2.5$ and $\sigma_b = 20$ for the TKE model. As the wave approximates the shore and shoals it is clear that the two models, as expected, give identical results since wave-breaking has not started yet. The breaking procedure starts around $t = 4.79sec$. Both the hybrid closure and the TKE model represent the solution as a triangular bore, albeit with a different resolution of the peak which is kept smoother and higher by the TKE approach. At time $t \sim 7.9sec$ the bore collapses on the shore and the wave starts to run-up. For this particular case both numerical solutions provide a good qualitative agreement with the data. We highlight here that the objective of this work is not so much related to which method best predicts the available data, but to provide some quantitative measures of the variability of the outputs wrt changes in the input parameters. In the current study, the variations of the flow quantities with numerical parameters, and more particularly mesh size, is not included. As already said, the interested reader is referred to the previous work [1, 16] for a detailed analysis of this aspect.

5.1 Model outputs and post-processing

An important point is the definition of the output observables to be used in the analysis. We will start by considering the sensitivities of the location of the breaking point, the wave height at the breaking point, the maximum wave height at the wave gauges and the maximum run-up.

To have a more detailed picture of the evolution of the wave as it shoals and breaks, we will also consider a set of statistical outputs. There exist several works that examine them in the context of BT models, see for example [8, 17, 38]. A measure to examine the left-right differences in a wave is the wave asymmetry which

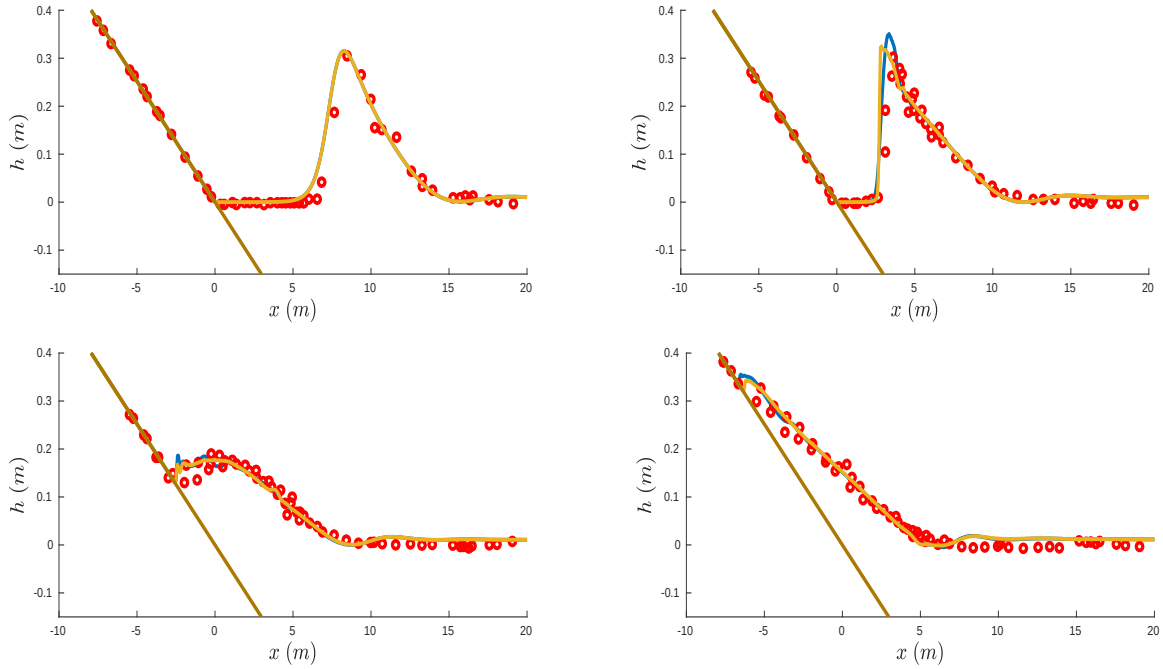

Figure 3: Time evolution of the free surface (deterministic). Yellow line: Hybrid wbc, blue line: TKE wbc.

is defines as

$$As = \frac{< H(\eta^3) >}{< \eta^2 >^{3/2}} \tag{17}$$

where H is the Hilbert transformation and $< \cdot >$ denotes the mean operator. A similar information is provided by wave skewness, which is a measure of crest-trough shape. It is defined as

$$Sk = \frac{< \eta^3 >}{< \eta^2 >^{3/2}}. \tag{18}$$

Finally, the kurtosis will allow to estimate whether the wave is heavy tailed or light tailed with respect to the normal distribution. It is defined as

$$Ks = \frac{\frac{1}{n}\sum (\eta_i - < \eta >)^4}{\left(\frac{1}{n}\sum (\eta_i - < \eta >)^2\right)^2} \tag{19}$$

where n is the length of the time series data in the wave gauge.

Finally, we will look in more detail into the impact of the physical set up parameters on the variability of maximum runup, allowing to compare with some of the data provided in [35].

5.2 Parameter sensitivity analysis

Besides the variations in the physical parameters already discussed, we consider uncertainties in the parameters of the models, involved in the detection (γ and θ) for both models and the energy dissipation for the TKE model ($\kappa,\ C_v,\ \sigma$). In particular we assume the the uniform distributions $\gamma \in [0.3,\ 0.8],\ \theta \in [0.32,\ 0.6]$ and $\kappa \in [0.5,\ 2.5]$, $C_v \in [5,\ 15]$, and $\sigma \in [10,\ 25]$. Note that the last three parameters appear only in the TKE model.

Figure 4 presents the First and Total order Sobol indices for the physical outputs, including the results in wave gauges. The results indicate that the amplitude of the wave is mainly the dominant parameter for the maximum wave height at the wave gauges and on the location of the breaking point for the hybrid model while for the TKE, κ plays also a significant role in the formation of the maximum wave height at the wave gauges offshore. As expected, and for both models, friction affects the maximum wave height at $x = 0m$, which is located on the initially dry slope. The parameter γ affects the location of the breaking point in the hybrid wbc but surprisingly plays no role in the TKE. An interesting outcome is the one of the runup process. Only the physical parameters are those who affect the maximum runup with the slope of the topography affecting only the hybrid wbc. We have to highlight here that all the second order Sobol indices are less that 0.1 (not shown). This indicates a small correlation between input parameters.

So, as a general conclusion we can say that the model parameters have a significantly smaller impact on the outputs than the problem setup parameters, with the exception of γ that does affect the breaking point location when using the hybrid wbc and κ that affects the maximum wave hight on the wave gauges. Among the problem parameters, the amplitude turns out to be the dominating one, followed by the friction. The slope has a somewhat smaller impact on the runup and that too only for the hybrid closure. To go further we look at the statistical parameters of the water elevation signals in the gauges. The results are summarized in figures 5 and 6 for the hybrid and the TKE wave breaking closures respectively. Wave amplitude, slope, and friction coefficient have the largest impact, while the indices of γ and θ are close to zero and they are not presented. When using the TKE model the only model parameter that shows sensitivity is κ and this only for the kurtosis. The asymmetry is largely controlled by the amplitude. This is especially true in the first gauges, close to the collapse of the wave (impact of amplitude), and to the runup/backwash (slope). The slope shows bigger sensitivity when the TKE closure is used.

Skewness and kurtosis present a different sensitivity profile for the two models revealing the different way of simulating propagating bores since the hybrid model represents the solution as a triangular bore with a sharp front and TKE as a bore with a smother and higher peak. When we use the hybrid wbc the skewness is highly affected by the amplitude as the wave breaks and collapses on the slope (first gauges). The impact of the slope and the amplitude are equally dominating the shoaling phase, with friction playing a smaller but not a negligible role. For the TKE wbc the behavior of the parameters are more clear since only the wave's amplitude and friction are dominating the process. The impact of the slope is only visible as the wave collapses on the slope.

The thickness of the wave tails, measured by the kurtosis, is controlled mainly by slope and friction as sown in figure 5 on the right. The first has a much higher sensitivity in the intermediate gauges suggesting that its impact is related to the propagation, while the impact of the friction more to the backwash. The results show that for the hybrid closure model the wave-breaking parameters have considerably smaller contributions to the shape of the wave. Finally the kurtosis, when we use the TKE wbc, is dominated by the wave's amplitude and the slope but also κ sows some sensitivity. We recall that κ controls both the magnitude of the eddy viscosity as well as the dissipation of turbulent kinetic energy. The latter may affect the rate at which the eddy viscosity is reduced in space, thus affecting the wave tail

5.2.1 Discussion on the convergence of the sensitivity indices

One of the main questions that can arise in this study is how the results are changing with respect to the numerical resolution. The answer to this question is twofold. The first aspect concerns the change of the physical output as the mesh is refined and is largely covered in [16]. We briefly report that the study performed in [16] has involved a systematic analysis of the behavior of the two closures for different mesh sizes, the study of dynamics of breaking through dissipation monitors. Thorough evidence of the equivalent

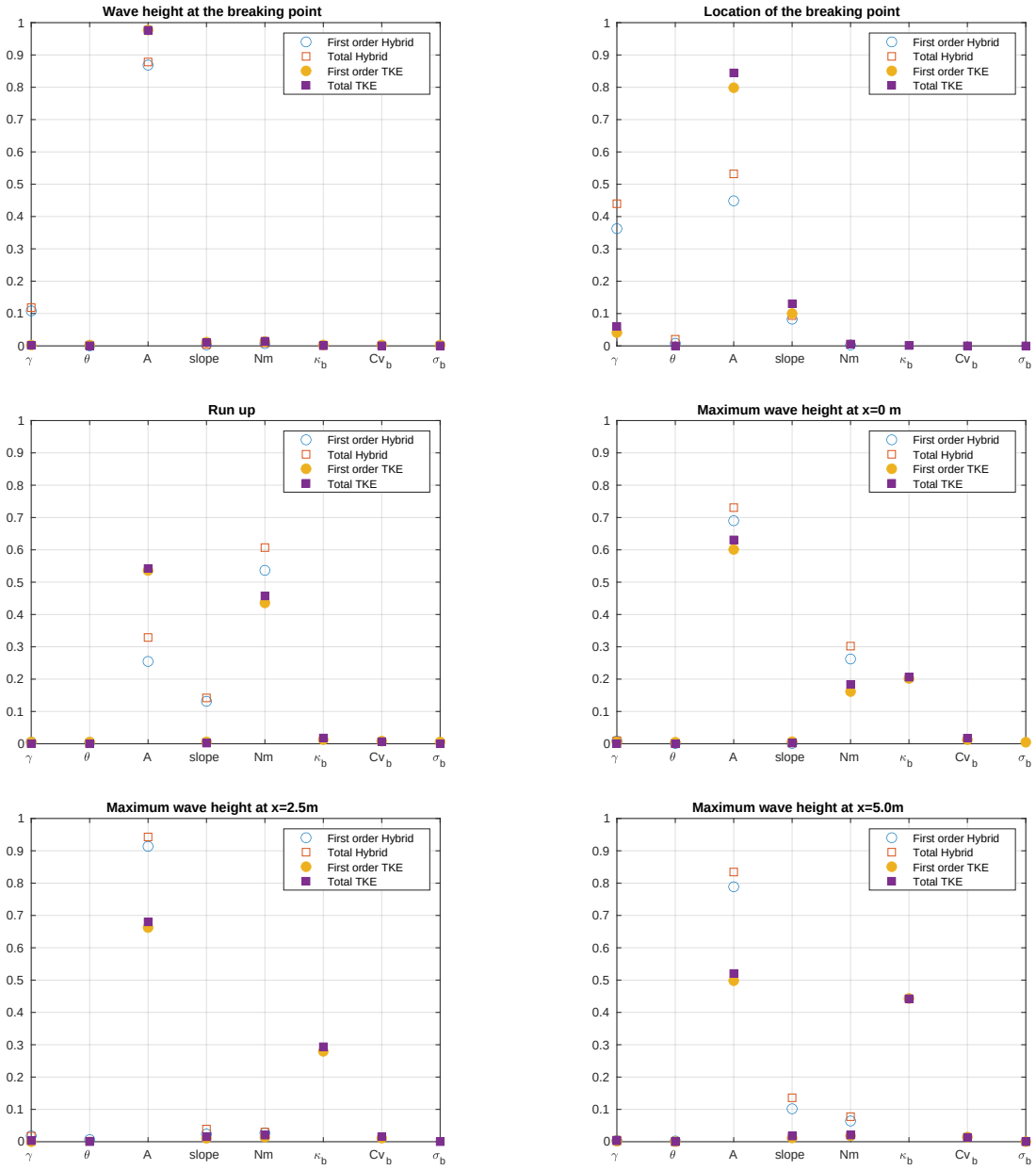

Figure 4: First (circles) and Total(squares) Sobol Indices for the output parameters using the hybrid and TKE (squares) wbcs.

capabilities of the two approaches to provide satisfactory results has been given. The results indicate that both closure approaches allow to describe correctly wave breaking at large scales and when we use the TKE the numerical dissipation plays a negligible role. The results also shown a reduced sensitivity to the mesh of this approach compared to the hybrid one.

The second issue that arises is the convergence of the statistical outputs as the mesh is refined. We investigate here this aspect by considering the variations of the statistics on four different meshes of sizes $\Delta x \in [0.05,\ 0.025,\ 0.025,\ 0.0125m]$. Note that in this analysis we made sure that on each mesh the metamodel

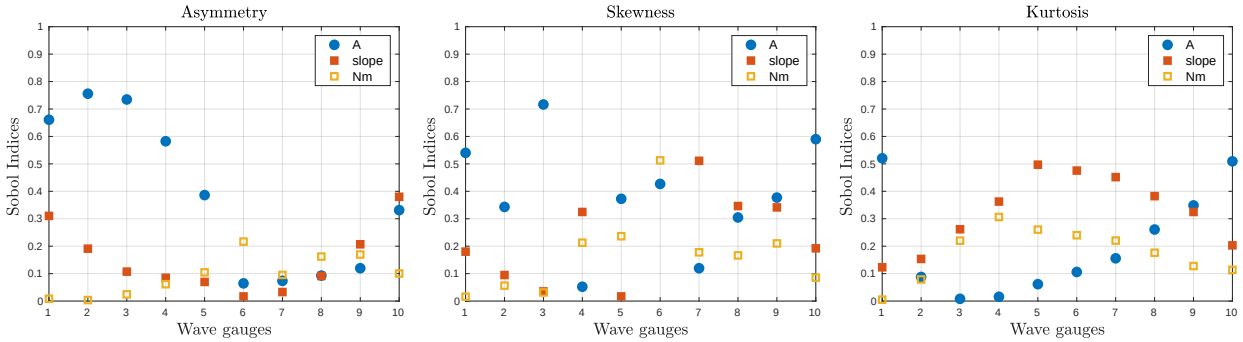

Figure 5: First order Sobol indices for Asymmetry, Kurtosis and Skewness measured on the wave gauges using the hybrid closure.

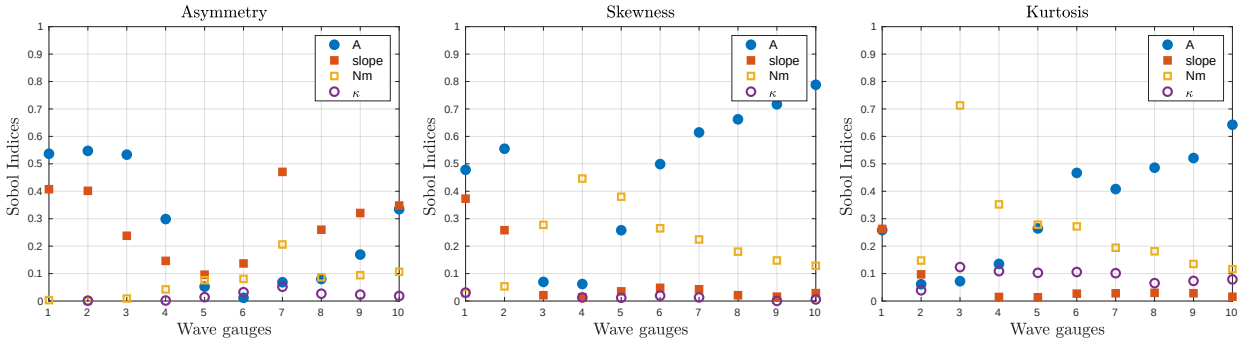

Figure 6: First order Sobol indices for Asymmetry, Kurtosis and Skewness measured on the wave gauges using the TKE closure.

built for the sensitivity analysis has converged in terms of number of samples for each output value and for each mesh.

Figure 7 presents the sensitivity indices for the four output parameters, the wave hight and the location on the breaking point, and the maximum wave hight at the wave gauges at $x = 2.5m$ and $x = 5.0m$. The input parameters of the closures are varied within 50% of their initial value. We plot only the indices that are more than 0.1. As expected, for the hybrid wbc the indices are almost constant for the coarser meshes while they start to diverge when the mesh is finer. As explained in [16] for finer meshes, and when we use the hybrid model, abrupt and spurious oscillations are introduced at the interface between the breaking and the nonbreaking region. This of course spoils the solution and consequently affects the sensitivity analysis. On the other hand when using the TKE wbc, the indices are almost the same for all the different discretizations proving that the solution is not changing when we vary the input parameters of the closure.

5.2.2 Sensitivity analysis with respect to runup

One of the most relevant outputs for risk assessment is the maximum runup. It is well understood that waves with higher amplitudes have higher impact on the coast, or in other words higher maximum runup. To investigate this, we look at the variability of the latter with respect to physical parameters. The maximum run-up as a function of the wave's amplitudes (for fixed slope=$1/19.85$, $Nm = 0.01$) is reported in the leftmost pictures in Figure 8 for both wave breaking closures. For comparison, the experimental data [35] are also plotted. We also report in the figure the dependence of the maximum runup on the slope (for fixed

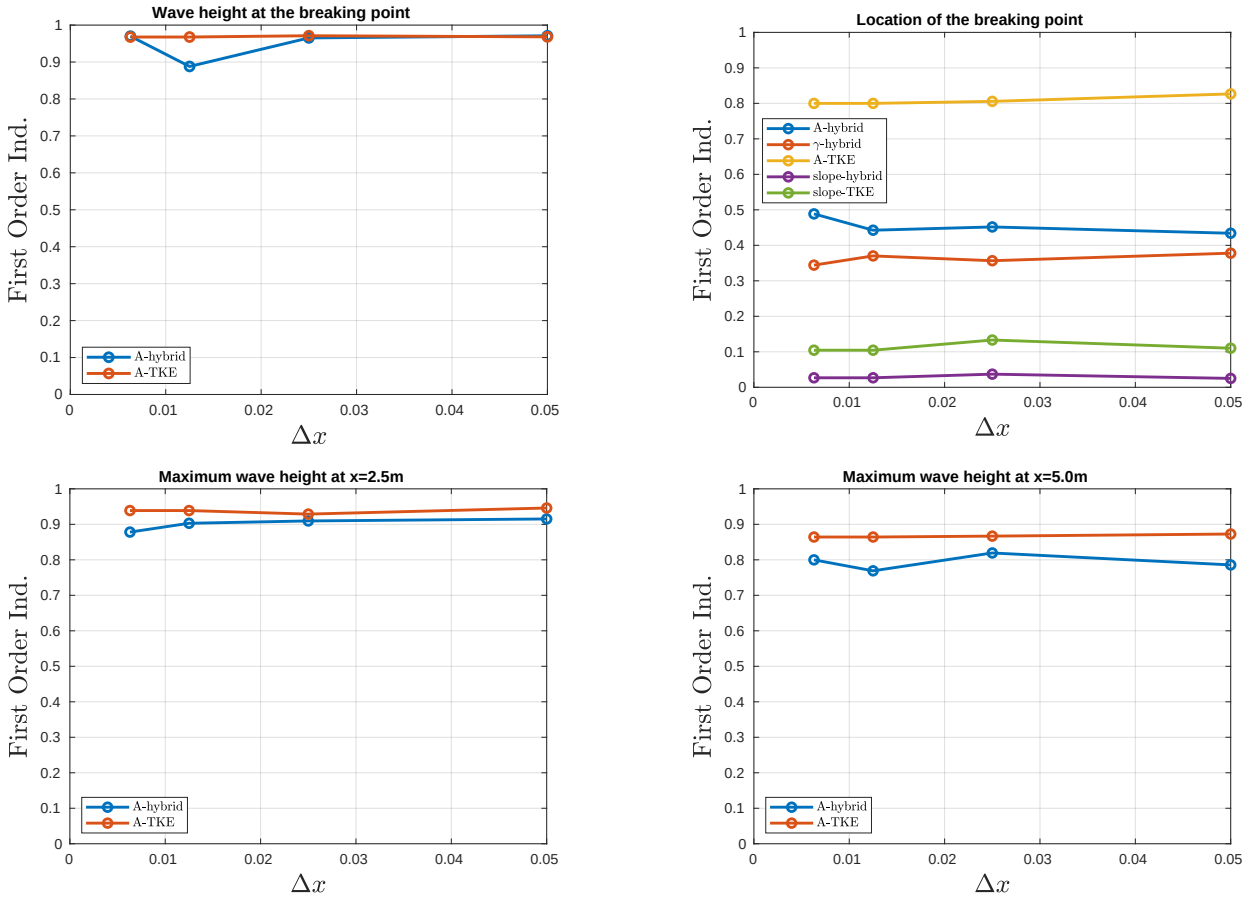

Figure 7: Sensitivity indices using different meshes for both closures.

$A = 0.28$ and $Nm = 0.01$),and on the Manning coefficient (for fixed slope=$1/19.85$ and $A = 0.28$). The metamodel predictions for different values of the wave breaking parameter γ are plotted.

Above the amplitude ~ 0.15 the maximum run-up increases almost linearly with A. The metamodel predictions are quite close to the data. For the hybrid wbc, the impact of the wave breaking parameter γ is not uniform over the range of amplitudes. Relevant variations of runup are only observed for intermediate values of A, when sensibly reducing γ (early breaking), and for the highest amplitudes when delaying too much the detection (highest values of γ). The local maximum variations of runup observed are of the order of ∼5-7%, the predictions remaining relatively close to the experimental data.

In the same spirit we fix the TKE closure by setting $\kappa = 0.5$, $C_\nu = 5.0$, $\sigma = 10.0$, and evaluate the impact of γ, of the slope and of the friction coefficient. The plots obtained are reported at the bottom of figure 8. For the amplitude dependence, we see that the match with the data in the plot against the dependence is very good. We also note a behavior much different than the one of the hybrid closure. In accordance to the sobol indices presented in the previous section we confirm that, for the present closure the wave breaking detection has virtually no effect.

The variability of the runup with the slope and the Manning has however a different behavior, for the hybrid closure. When lowering the value of the detection parameter (early breaking), we see a systematic impact of the order of $\sim$ 9-10% over the entire range of slopes. A weaker dependence on the slope is observed when using the TKE closure.

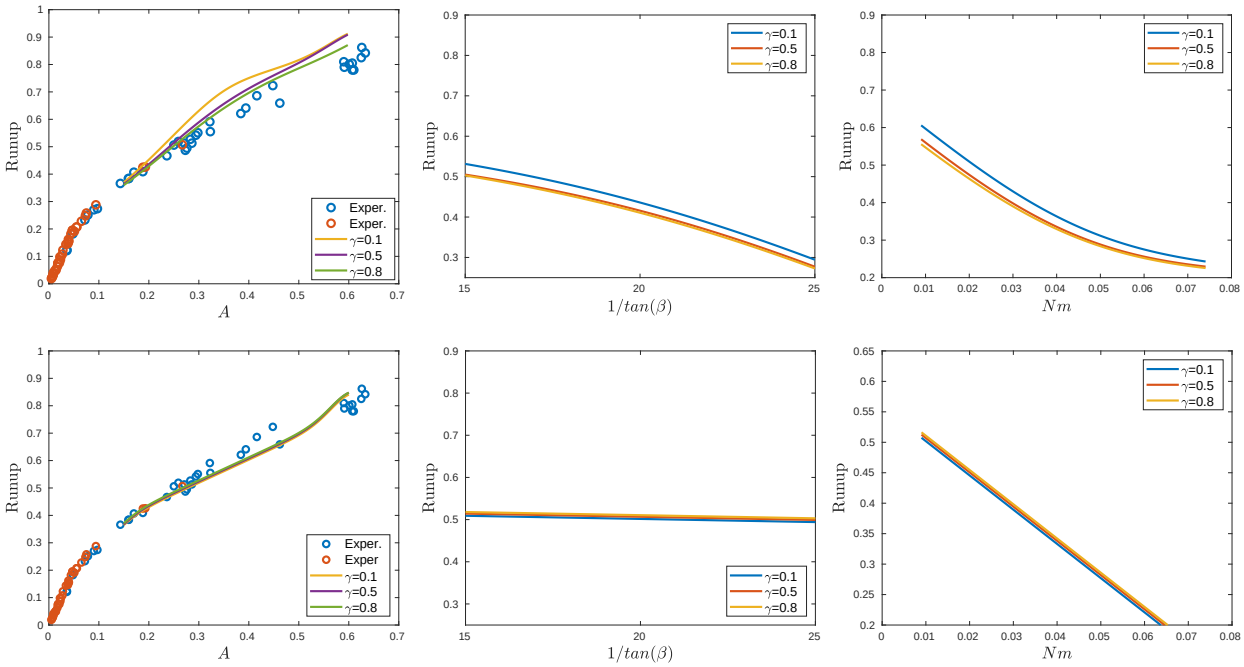

Figure 8: Run up as a function of wave's amplitude were slope=$1/19.85,\ Nm = 0.01$ (left), of slope were $A = 0.28,\ Nm = 0.01$ (center) and of the Nm number were slope=$1/19.85,\ A = 0.28$ (right). Using the hybrid (up) and the TKE (down) wave breaking closures.

A similar, to the variability of the runup with the slope, trend is observed, for the hybrid model, when looking at the dependence with the Manning coefficient. The lowest value of the parameter γ leading consistently to variations of the runup of the order of the maximum observed when changing the amplitude. This suggests that the runup may be more tolerant to some input error on the wave amplitude, while the correct parametrization of the breaking detection for the hybrid closure is more crucial when we have uncertainties in the slope and friction. The runup dependence on the Manning coefficient for the two closures is very similar.

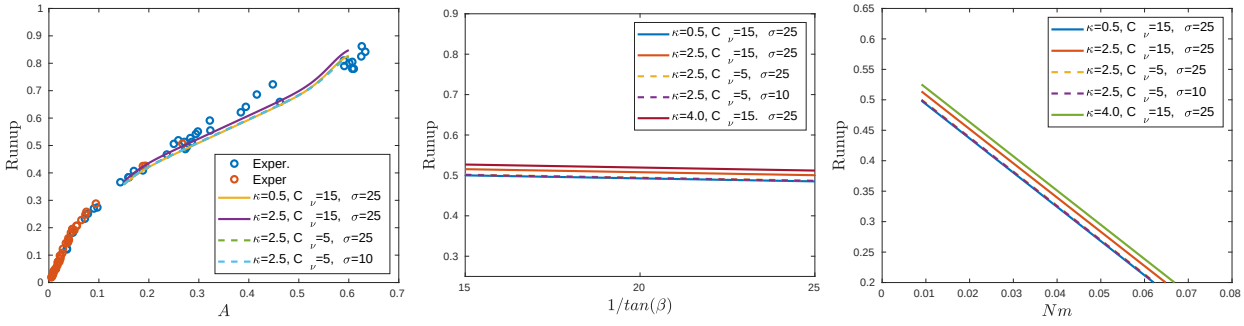

Figure 9: Run up as a function of wave's amplitude were slope=$1/19.85,\ Nm = 0.01$ (left), of slope were $A = 0.28,\ Nm = 0.01$ (center) and of the Nm number were slope=$1/19.85,\ A = 0.28$ (right).

Finally and for the TKE, we fix $\gamma = 0.6$ and vary the other input parameters. The resulting behavior

is the one reported on Figure 9. Again we see a secondary and almost negligible impact of the model parameters on the runup. This is quite interesting as it means that the value predicted is quite robust with respect to the parametrization of the wave breaking, and mostly controlled by the problem setup.

5.2.3 A solitary of $\epsilon = 0.28$ over a slope

For completeness we now focus on the impact of the model parameters alone, for the fixed nominal values of the physical parameters: $A = 0.28$, slope=$-1/19.85$ and $Nm = 0.01$. For the hybrid closure, we are left only with the γ and θ parameters controlling wave breaking detection, and we have seen already that the first has a dominant contribution to output variations in the general case. As usual for the second wave breaking closure we have both the initiation and diffusive parameters that control the analysis. Figure 10 shows the first and total Sobol indices for some of the examined outputs. We can see that breaking detection, and in particular γ, has a major impact on the maximum wave heights. Large contributions to the variance also come from κ and C_ν, which in particular are the only dominating parameters for the run-up. We see here also a non-negligible difference between some first and Total indices, indicating the presence of some important interactions on the maximum wave's height. More precisely at WG 1 ($x = 0m$) and WG 6 ($x = 2.5m$) the second order index for γ and κ is 0.17 and 0.109 respectively.

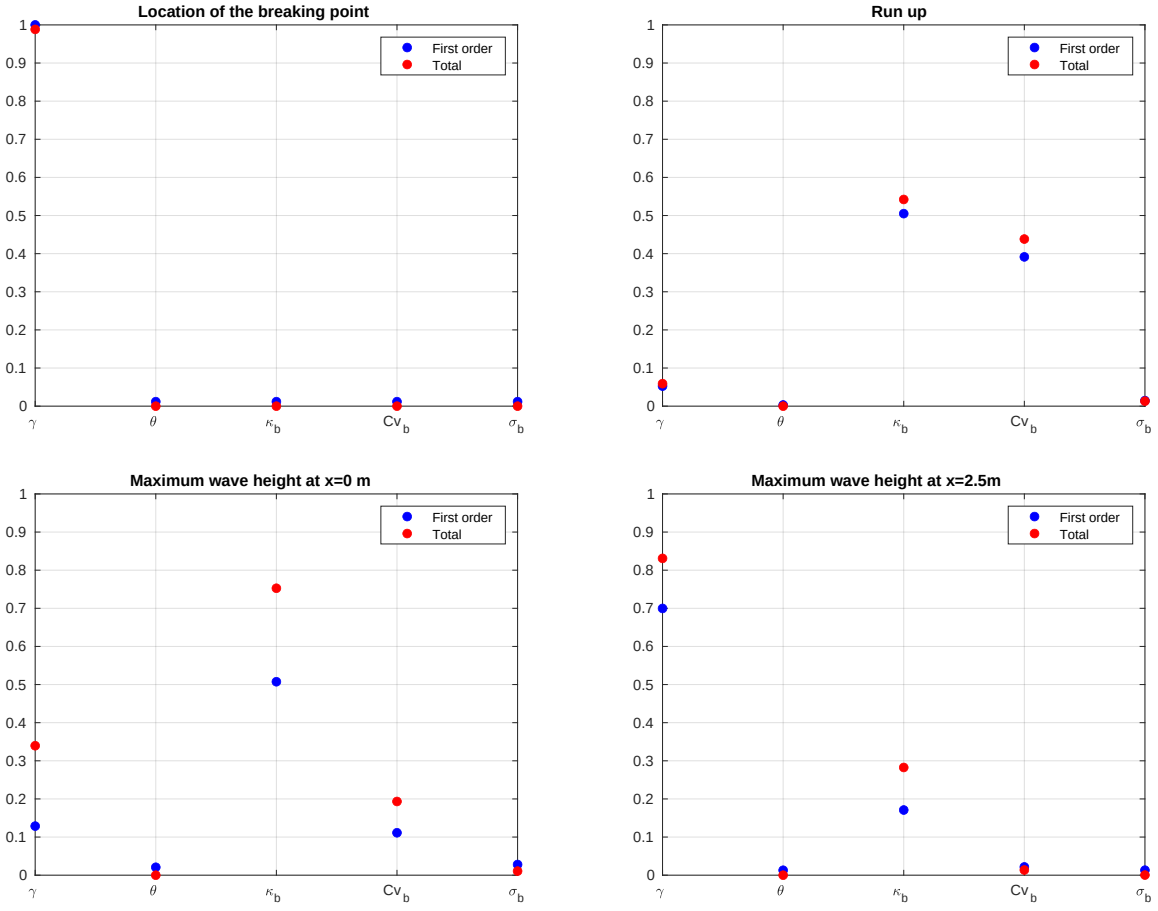

Figure 10: First (blue) and Total (red) Sobol Indices for the run-up and the maximum wave height at WG1 and WG6 using the TKE wbc.

5.3 Pointwise spatial distributions and temporal evolutions of sensitivities

For fixed values of the problem parameters, we see a similar behaviour of the Sobol indices in Figure 11 for the wave moments in the wave gauges. The γ parameter is responsible for almost 100% of the variance, except in the intermediate regions (breaking area), and in the last gauge. For the TKE, in Figure 12, wave's asymmetry and kurtosis are affected mainly by the parameters κ and C_ν, i.e. from the dissipation and production term in the transport equation 6. On the other hand, skewness, i.e the crest to trough shape, is mainly affected by C_ν which probably controls the kinetic energy cutoff before and after the breaking front.

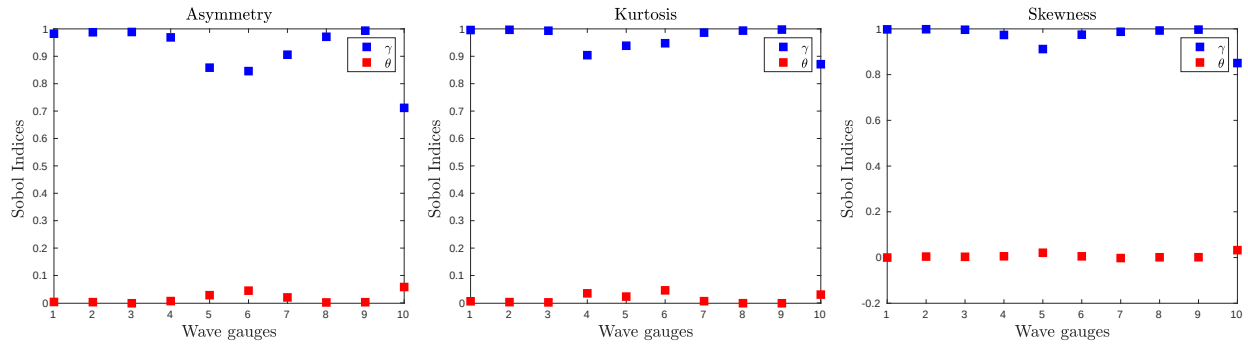

Figure 11: First order Sobol indices for Asymmetry, Kurtosis and Skewness measured on the wave gauges, when $A = 0.28m$.

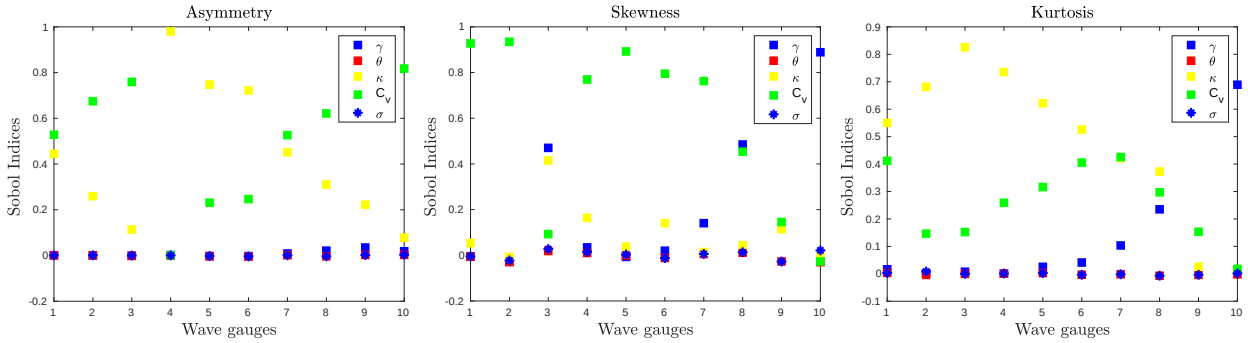

Figure 12: First order Sobol indices for Asymmetry, Kurtosis and Skewness measured on the wave gauges.

To try to understand how θ still affects the solution, we report on Figure 13 the variance of dimensionless outputs for fixed values of γ for the hybrid closure. More precisely, the wave height at the breaking point (whbp) and the maximum height for the wave (mwh) at $x = 0,\ 2.5,$ and $3m$ are scaled by the initial amplitude of the wave, and the location of the breaking point (bp) is scaled by the initial position of the solitary. Finally, the run-up values are scaled by the experimental values for the specific case. We see that variations above 1% are only observed for the position of the breaking point, and for the maximum wave height at breaking point and at $x = 2.5$, corresponding to the initial shoreline. In particular, for all these outputs we see a clear increase variance above a certain threshold of γ. This is the sign that above this value breaking detection is related to the second criterion. This is visualized in the right picture on the figure showing the variation of the position of the breaking point with γ for different samples of the metamodel. Above a critical value of γ this position only depends on θ.

To have a better insight we study the evolution of the water depth in the whole domain in space by freezing the time in specific characteristic time spots. This means that we look at the spatial evolution of the

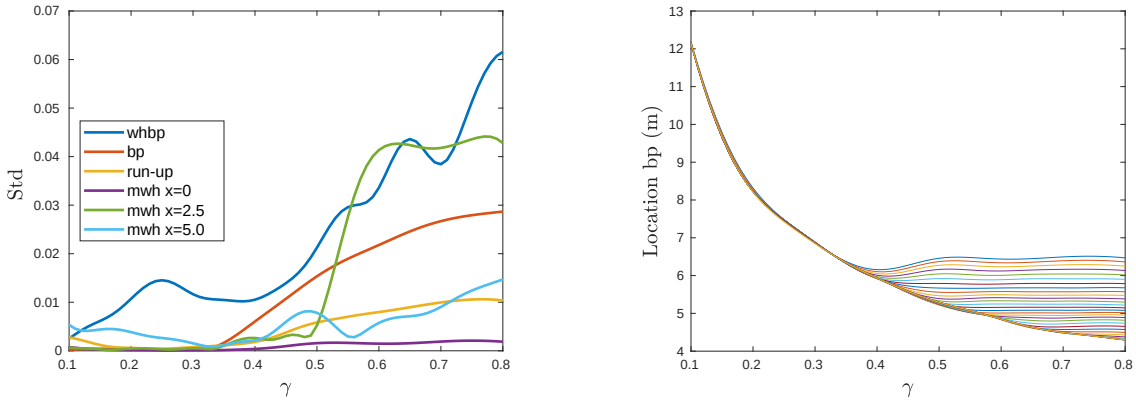

Figure 13: Standard deviation for the output parameters in respect to gamma (left) and evolution of the location of the bp.

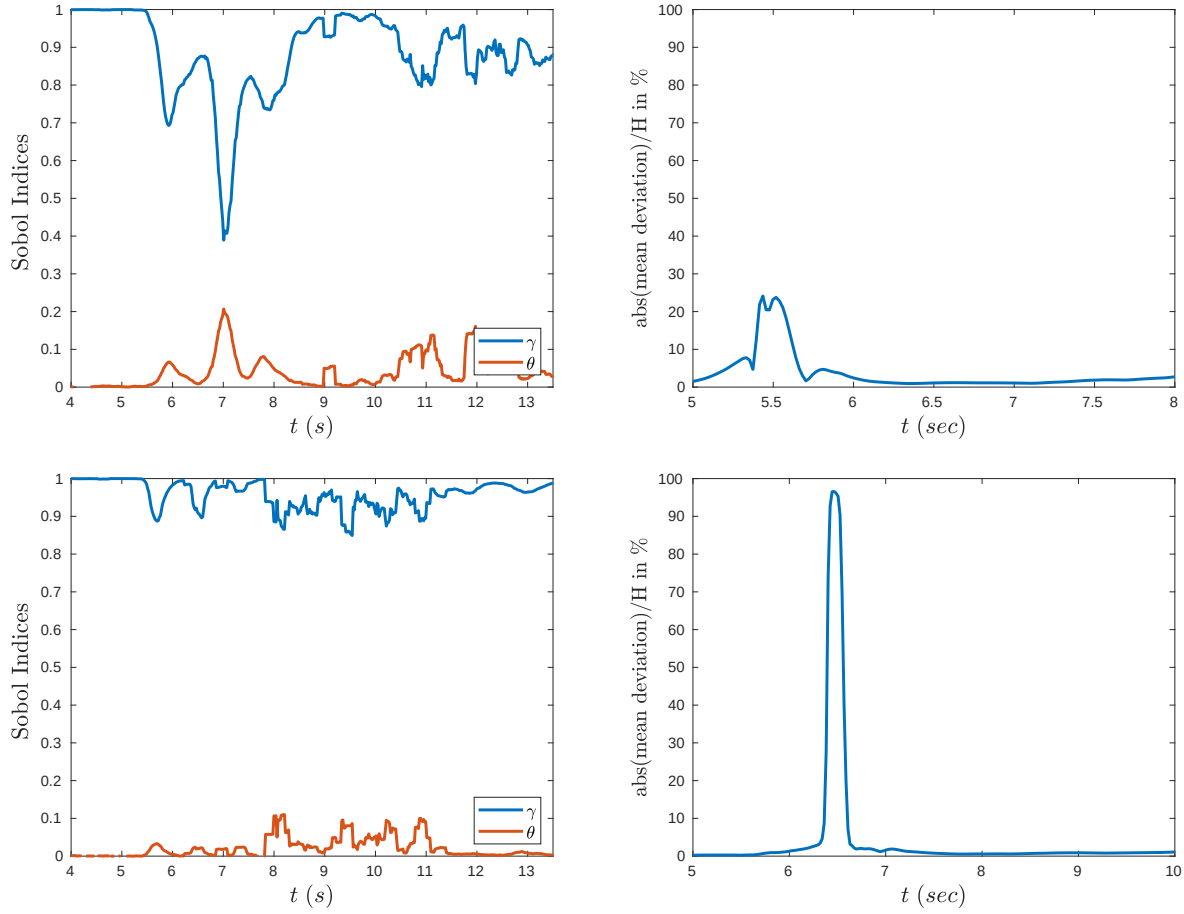

Figure 14: Temporal evolution of the First Order SI and deviation of the free surface elevation, at WG10 and WG 6.

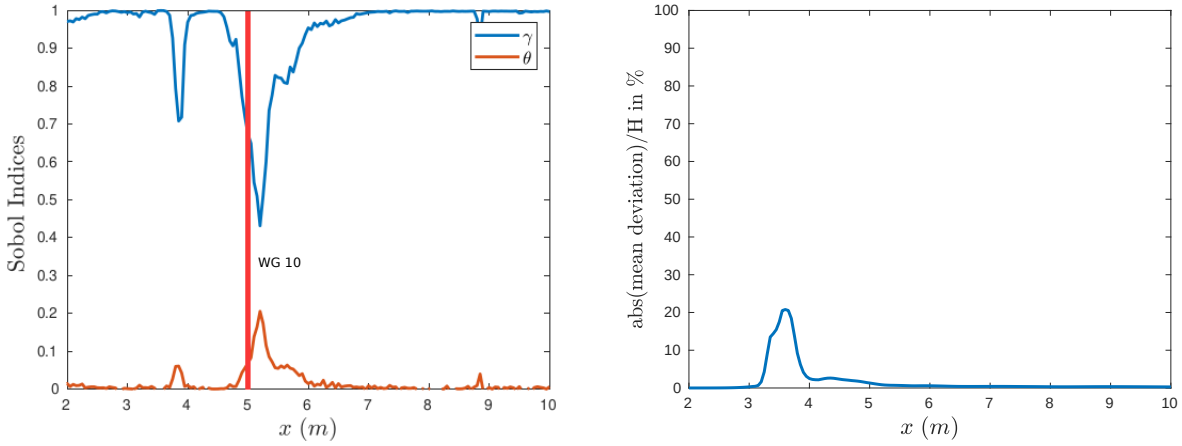

Figure 15: Spatial evolution of the First order SI and the deviation of water depth at $t = 6.0sec$.

sensitivity indices of the free surface elevation, shown in the left plot in Figure 15. The spatial distribution is computed at $t = 6.0sec$, i.e. during the breaking process. Red line denotes the location of the closest wave gauge, i.e. WG 10. Since γ is the dominant parameter in the whole domain we want to check where exactly it plays a crucial role, that is why we plot right next to the figure the absolute mean deviation of the water depth over the water depth, at $t = 6sec$. We observe that the maximum mean deviation is 25%, compered to the mean water depth, and occurs between $3m$ and $4m$. After this region the deviation is less than 5%, so γ is still the dominant parameter but in negligible changes of the water depth. The temporal distribution 14 of the sensitivity indices is computed for the free surface elevation recorded at WG10 ($x = 5.0m$) and WG6 ($x = 2.5m$). Like before, θ is not the dominant parameter while the bore is breaking. To confirm how much it contributes we plot again the deviation of the free surface elevation. We can see that the maximum deviation grows as the wave propagates on shore reaching more than 90%, meaning that mainly γ is affecting the bore front.

We perform the same exercise but for the TKE closure. In 16 we report the spatial evolution of the water depth, sensitivity indices and absolute mean deviation of the water depth, at times representative of incipient $t = 6sec.$, and after collapsing on the shore ($t = 8.2sec$). Its clear that in the early breaking time γ and κ are the predominant parameters affecting the water depth until 6m in the domain. More precisely the deviation of the water depth compared to the mean water depth is maximum 2.5%. This shows the robustness of the TKE model in contrast to the hybrid where the maximum deviation at the same time is 25%. After the collapse of the bore on the shore κ and C_v are taking the lead and strongly affect the free surface elevation especially, the front of the wave. This is confirmed by the absolute mean deviation of the water depth shown in the low right figure of 16.

Next we study their temporal evolution in the wave gauges. For WG 10 the absolute mean deviation is almost zero, meaning that the parameters are not affecting the evolution of the free surface elevation. We report in Figure 17 , and for the sake of completeness the results for WG6. The absolute mean deviation reaches almost 40% within the time interval 6 to 7seconds where the most important parameters are κ and C_ν. A consistent behavior is observed in all the WG's verifying that the wave-breaking mechanism is "following" the wave as it breaks until its collapse on the shore.

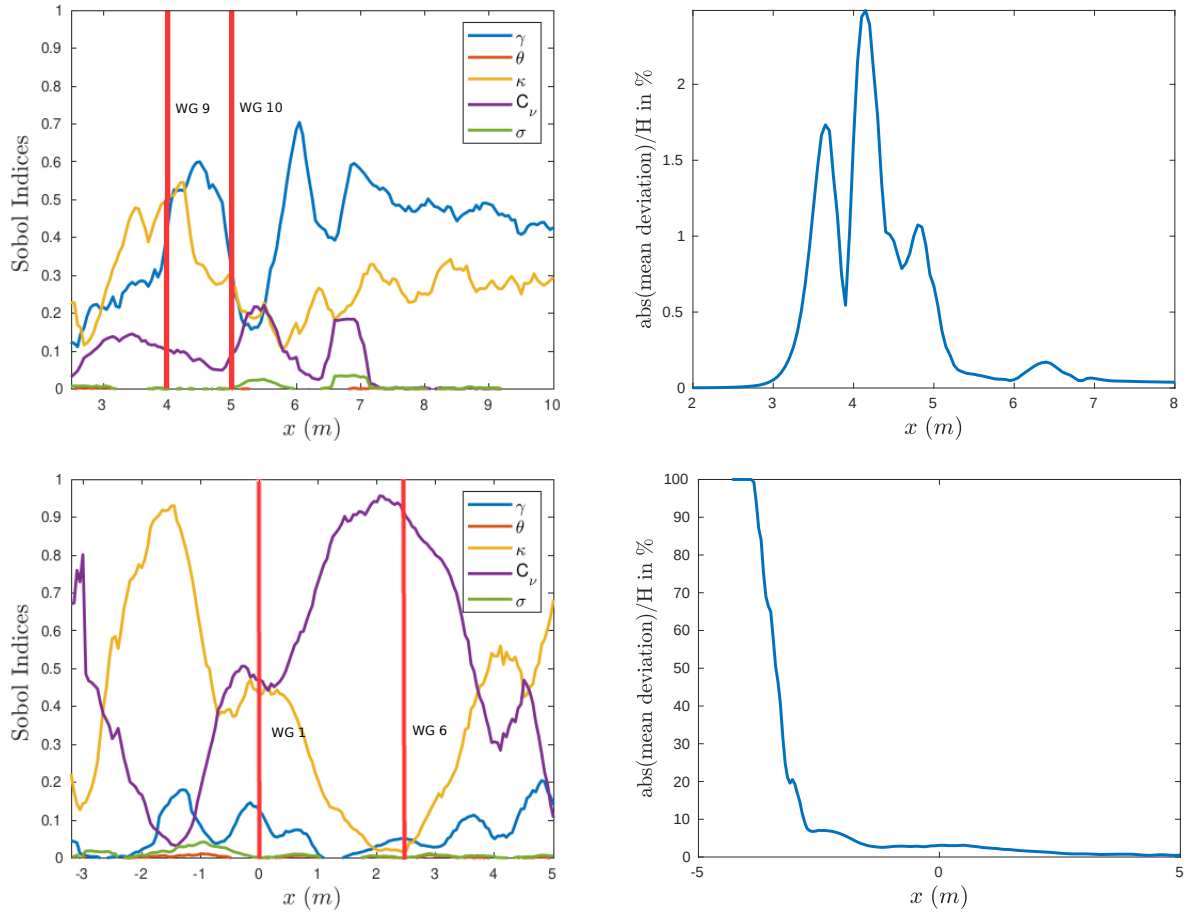

Figure 16: Spatial evolution of the Sobol indices and the absolute mean deviation for $t = 6,\ 8.2sec$.

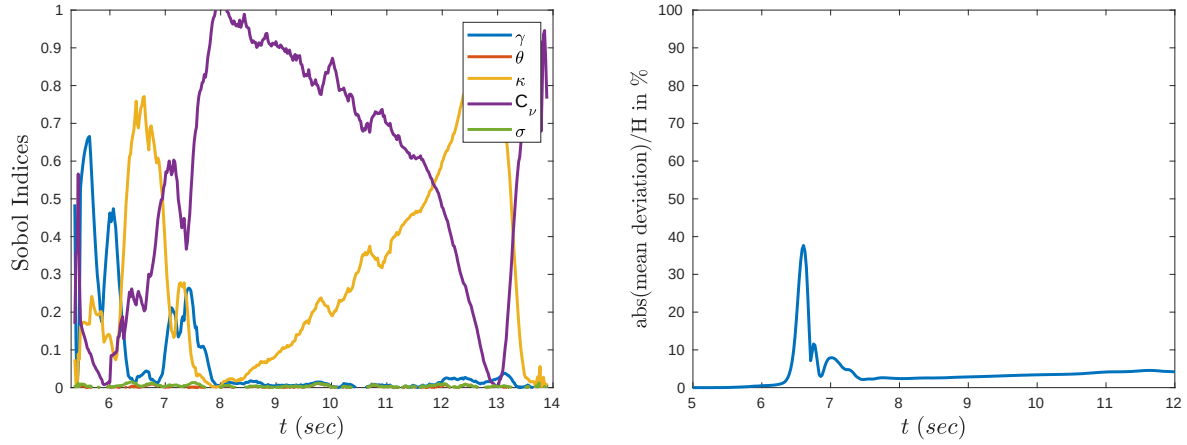

Figure 17: Temporal evolution of the Sobol indices and the absolute mean deviation of the free surface at WG6.

6 Summary of the results and comparison of the two breaking closures

We conclude that, for the hybrid model, the initial amplitude of the wave is the most dominant parameter corresponding to almost every output metric before the run-up. The shape of the wave depends on the initial amplitude, and also on the slope of the beach during the run-up. The kurtosis of the wave is affected by mostly the slope of the beach and the friction coefficient. For the hybrid model, the statistical metrics are most affected by the wave-dependent input parameters. Among the model-specific parameters such as γ and θ, the former one has the most effect on the statistical metrics, more so after the value of $\gamma > 0.3$. θ, although not a dominant parameter for wave breaking, does contribute to the tail of the wave post breaking.

For the TKE model, the Sobol indices indicate that the wave amplitude is the most dominant parameter for the deterministic metrics, similar to the hybrid model. However, when the amplitude and the slope values are fixed, it emerges that κ and Cv are the parameters which most affect the output metrics.

It is also seen that, among the two candidate models, the hybrid model shows a significant effect of γ on the run-up of the wave, in contrast to the TKE model, which shows almost no effect of changes in γ. Further, in the case of the hybrid model, the effect of γ is less sensitive to changes in the initial amplitude when the slope and the friction parameters are fixed. This implies that, when using the hybrid model, small errors in the slope or the friction parameters may manifest into considerable errors in the prediction of the maximum run-up. On the other hand, the TKE model doesn't show a similar effect of γ on the run-up process over a range of values for the initial amplitude, friction and the slope parameters. However, once we fix the value of γ, the predicted run-up of the waves reflects a larger influence of the friction and the slope parameters compared to the initial amplitude of the wave when the TKE model parameters are varied. Thus, it can be concluded that the run-up predicted by either of the models may be more sensitive to the errors in the measurement of the friction or the slope parameters, in comparison to the initial amplitude of the waves, and will depend on the choice of γ for the hybrid model and the model parameters for the TKE model.

Finally, the absolute mean deviation of the free surface elevation measured at the wave gauges reveals that the hybrid model can lead to large differences between the observed values of the free surface elevation and the mean free surface elevation, up to 90%. On the other hand TKE model is more robust mainly on the off-shore region.

We have to note the differences of the Sobol indices for the statistical parameters between the two wave-breaking closures, see Figure 5 and 6. This is due to the fact that the wave-breaking closures simulate the breaking wave in a different way. The hybrid closure simulates the breaking wave as a traveling bore while the one obtained using the tke closure has a smoother propagating front.

7 Conclusion and perspectives

In this work, we systematically analyse the effect of various parameters on the performance of two models for wave breaking. In particular, we perform the Analysis of Variance (ANOVA) which gives First and Total-order Sobol's indices, which in turn quantify the sensitivities of specified output metric on the input parameters. We first obtain a Gaussian Process Regression metamodel of the high-fidelity CFD model prior to performing the ANOVA analysis. We quantify the sensitivities using several deterministic metrics such as the maximum height of the wave, the location of the breaking of the wave, the maximum run up, the time-series values at several gauges, as well as stochastic metrics such as the skewness, asymmetry and kurtosis of the time-series of the wave at several gauge locations. We study different configurations of the classical problem of the solitary wave run-up on a slope. We also study the time-evolution of the Sobol indices at specific gauge locations. The importance of this analysis is twofold. First, it helps us gain

insights into physics of nonlinear and dispersive waves, specifically during the breaking and the run-up phases. Secondly, it quantitatively distinguishes between the two prominent approaches for modeling the breaking of the waves, viz. the hybrid method and the TKE model for wave breaking.

Compliance with ethical standards

There is no conflict of interest. Data sharing is not applicable to this article as no datasets were generated or analyzed during the current study.

References

[1] Paola Bacigaluppi, Mario Ricchiuto, and Philippe Bonneton. Implementation and evaluation of breaking detection criteria for a hybrid boussinesq model. Water Waves, 2019.

[2] X Barthelemy, ML Banner, WL Peirson, F Fedele, M Allis, and F Dias. On a unified breaking onset threshold for gravity waves in deep and intermediate depth water. Journal of Fluid Mechanics, 841:463–488, 2018.

[3] Iooss Bertrand and Lemaître Paul. A review on global sensitivity analysis methods. Operations Research/ Computer Science Interfaces Series, 59:101–122, 2015.

[4] P. Bonneton. Modelling of periodic wave transformation in the inner surf zone. Ocean Engineering, 34(10):1459 – 1471, 2007.

[5] Philippe Bonneton, Florent Chazel, David Lannes, Fabien Marche, and Marion Tissier. A splitting approach for the fully nonlinear and weakly dispersive green–naghdi model. Journal of Computational Physics, 230(4):1479–1498, 2011.

[6] Maurizio Brocchini. A reasoned overview on boussinesq-type models: the interplay between physics, mathematics and numerics. Proceedings of the Royal Society A: Mathematical, Physical and Engineering Sciences, 469(2160):20130496, 2013.

[7] H. Chanson. Hydraulics of Open Channel Flow - 2nd Edition. 2004.

[8] Rodrigo Cienfuegos, Eric Barthélemy, Philippe Bonneton, and Xavier Gondran. Nonlinear surf zone wave properties as estimated from boussinesq modelling: random waves and complex bathymetries. In Coastal Engineering 2006: (In 5 Volumes), pages 360–371. World Scientific, 2007.

[9] Morteza Derakhti, James T. Kirby, Michael L. Banner, Stephan T. Grilli, and Jim Thomson. A unified breaking onset criterion for surface gravity water waves in arbitrary depth. https://arxiv.org/abs/1911.06896, 11 2019.

[10] Schulz Eric, Speekenbrink Maarten, and Krause Andreas. A tutorial on Gaussian process regression: Modelling, exploring, and exploiting functions. Journal of Mathematical Psychology, 85:1–16, 2018.

[11] Andrea Gilberto Filippini, Maria Kazolea, and Mario Ricchiuto. A flexible genuinely nonlinear approach for nonlinear wave propagation, breaking and run-up. Journal of Computational Physics, 310:381–417, 2016.

[12] Stephan T Grilli, Ib A Svendsen, and Ravishankar Subramanya. Breaking criterion and characteristics for solitary waves on slopes. Journal of waterway, port, coastal, and ocean engineering, 123(3):102–112, 1997.

[13] Shih-Chun Hsiao, Tai-Wen Hsu, Ting-Chieh Lin, and Yu-Hsuan Chang. On the evolution and run-up of breaking solitary waves on a mild sloping beach. Coastal Engineering, 55(12):975–988, 2008.

[14] Subodh Joshi, Maria Kazolea, and Mario Ricchiuto. Sensitivity analysis for two wave breaking models used by the green-naghdi equations. 14th World Congress on Computational Mechanics (WCCM) and ECCOMAS Congress 2020, 2021.

[15] M Kazolea, Argiris I Delis, and Costas E Synolakis. Numerical treatment of wave breaking on unstructured finite volume approximations for extended boussinesq-type equations. Journal of computational Physics, 271:281–305, 2014.

[16] Maria Kazolea and Mario Ricchiuto. On wave breaking for boussinesq-type models. Ocean Modelling, 123:16–39, 2018.

[17] Andrew B Kennedy, Qin Chen, James T Kirby, and Robert A Dalrymple. Boussinesq modeling of wave transformation, breaking, and runup. i: 1d. Journal of waterway, port, coastal, and ocean engineering, 126(1):39–47, 2000.

[18] C. Lataniotis, D. Wicaksono, S. Marelli, and B. Sudret. UQLab user manual – Kriging (Gaussian process modeling). Technical report, Chair of Risk, Safety and Uncertainty Quantification, ETH Zurich, Switzerland, 2019. Report # UQLab-V1.3-105.

[19] Randall J LeVeque et al. Finite volume methods for hyperbolic problems, volume 31. Cambridge university press, 2002.

[20] Yok Sheung Li and JM Zhan. Chebyshev finite-spectral method for 1d boussinesq-type equations. Journal of waterway, port, coastal, and ocean engineering, 132(3):212–223, 2006.

[21] Pengzhi Lin, Kuang-An Chang, and Philip L-F Liu. Runup and rundown of solitary waves on sloping beaches. Journal of waterway, port, coastal, and ocean engineering, 125(5):247–255, 1999.

[22] Sobol I. M. Sensitivity estimates for non linear mathematical models. Mathematical Modelling and Computational Experiments, (1):407–414, 1993.

[23] Sobol I. M. Global sensitivity indices for nonlinear mathematical models and their Monte Carlo estimates. Mathematics and Computers in Simulation, 55:271–280, 2001.

[24] S. Marelli, C. Lamas, K. Konakli, C. Mylonas, P. Wiederkehr, and B. Sudret. UQLab user manual – Sensitivity analysis. Technical report, Chair of Risk, Safety and Uncertainty Quantification, ETH Zurich, Switzerland, 2019. Report # UQLab-V1.3-106.

[25] Stefano Marelli and Bruno Sudret. Uqlab: A framework for uncertainty quantification in matlab. In Vulnerability, uncertainty, and risk: quantification, mitigation, and management, pages 2554–2563. 2014.

[26] Yue Ning, Weijie Liu, Zhilin Sun, Xizeng Zhao, and Yao Zhang. Parametric study of solitary wave propagation and runup over fringing reefs based on a boussinesq wave model. Journal of Marine Science and Technology, 24(2):512–525, 2019.

[27] Okey Nwogu. Alternative form of boussinesq equations for nearshore wave propagation. Journal of waterway, port, coastal, and ocean engineering, 119(6):618–638, 1993.

[28] Okey Nwogu and Zeki Demirbilek. Infragravity wave motions and runup over shallow fringing reefs. Journal of waterway, port, coastal, and ocean engineering, 136(6):295–305, 2010.

[29] Okey George Nwogu. Numerical prediction of breaking waves and currents with a boussinesq model. In Coastal Engineering 1996, pages 4807–4820. 1997.

[30] Philip L Roe. Approximate riemann solvers, parameter vectors, and difference schemes. Journal of computational physics, 43(2):357–372, 1981.

[31] Volker Roeber, Kwok Fai Cheung, and Marcelo H Kobayashi. Shock-capturing boussinesq-type model for nearshore wave processes. Coastal Engineering, 57(4):407–423, 2010.

[32] Andrea Saltelli. Making best use of model evaluations to compute sensitivity indices. Computer Physics Communications, 145(2):280–297, 2002.

[33] Hemming A Schäffer, Per A Madsen, and Rolf Deigaard. A boussinesq model for waves breaking in shallow water. Coastal engineering, 20(3-4):185–202, 1993.

[34] OR Sørensen, HA Schäffer, and PA Madsen. Surf zone dynamics simulated by a boussinesq type model. iii. wave-induced horizontal nearshore circulations. Coastal Engineering, 33(2-3):155–176, 1998.

[35] Costas Emmanuel Synolakis. The runup of solitary waves. Journal of Fluid Mechanics, 185:523–545, 1987.

[36] M Tissier, P Bonneton, F Marche, F Chazel, and D Lannes. A new approach to handle wave breaking in fully non-linear boussinesq models. Coastal Engineering, 67:54–66, 2012.

[37] Mara Tonelli and Marco Petti. Hybrid finite volume–finite difference scheme for 2dh improved boussinesq equations. Coastal Engineering, 56(5-6):609–620, 2009.

[38] Mara Tonelli and Marco Petti. Shock-capturing boussinesq model for irregular wave propagation. Coastal Engineering, 61:8–19, 2012.

[39] JA Zelt. The run-up of nonbreaking and breaking solitary waves. Coastal Engineering, 15(3):205–246, 1991.

[40] Yao Zhang, Andrew B Kennedy, Aaron S Donahue, Joannes J Westerink, Nishant Panda, and Clint Dawson. Rotational surf zone modeling for o (μ4) boussinesq–green–naghdi systems. Ocean Modelling, 79:43–53, 2014.

[41] Quan Zhou, Jie-Min Zhan, and YS Li. Parametric investigation of breaking solitary wave over fringing reef based on shock-capturing boussinesq model. Coastal Engineering Journal, 58(2):1650007–1, 2016.